PERGAMON International Journal of Solids and Structures 36 (1999) 575–595

INTERNATIONAL JOURNAL OF SOLIDS and STRUCTURES

On the axial propagation of kink bands in fiber composites: Part II analysis

S.-Y. Hsu, T. J. Vogler, S. Kyriakides*

Research Center for Mechanics of Solids, Structures and Materials, The University of Texas at Austin, WRW 110, Austin, TX 78712, U.S.A.

Received 13 August 1997; in revised form 12 January 1998

Abstract

A new micromechanical model is presented to simulate the steady-state axial propagation of kink bands investigated experimentally in the accompanying paper (Part I). The fibers are in a hexagonal array and are assumed to be isotropic and linearly elastic, while the matrix is modeled as an elastic-powerlaw viscoplastic solid. Matrix properties for the model are determined from shear tests on the composite and compression tests on neat PEEK. The model is used to predict the propagation stress (σ_P) of the AS4/PEEK composite and to investigate the sensitivity of σ_P to band inclination, matrix properties, and loading rate. A simple model recently reported in the literature is calibrated to the current material system and compared with the present experimental data and model predictions. The micromechanical model is found to predict the propagation stress reasonably well and to capture the rate dependence of the composite. The simple model is found to capture the trends of the behavior.

1. Introduction

The major characteristics of the phenomenon of quasi-static axial propagation of a kink band in an aligned fiber composite (AS4/PEEK) were discussed in Part I of this two part series using experimental measurements and observations. Here we present an idealized model of the phenomenon and use it to examine the sensitivity of the propagation stress to several of the parameters of the problem. The model is in the same spirit as the three-dimensional micromechanical model used in Hsu et al. (1998) to study the onset of failure of such composites. Whereas the emphasis there was on the prediction of the effect of small initial fiber imperfections on the onset of failure and of the localization events that follow, here we are concerned with the steady-state, quasi-static, axial propagation of a kink band already in place, that is, after it has been initiated. In Hsu et al. we idealized the composite as a hexagonal array of circular, elastic

* Author to whom correspondence should be addressed.

0020-7683/99/$ - see front matter
PII: S0020-7683(98)00030-4

fibers surrounded by an elasto-plastic matrix. This geometric idealization is also adopted here, but, in view of the added complication of the rate sensitivity of the propagation stress demonstrated in the experiments, the matrix is now modeled as an elastic-powerlaw viscoplastic solid. The performance of this model will be evaluated by direct comparison with the experimental results in Part I.

Budiansky et al. (1997)[I] recently developed a simple model for steady-state kink band broadening.[1] We will calibrate it to our material constants and evaluate its performance vis-á-vis the experimental and numerical results of the present study.

2. Analysis

2.1. *Model domain and discretization*

The hexagonal distribution of fibers used in the composite model is shown in Fig. 1(a). The fibers are assumed to be circular with diameter h and to have a spacing that corresponds to a fiber volume fraction (v_f) of 0.60. Figure 1(b) shows a characteristic cell of the material which will be used to calibrate the constitutive model described below. The width of the cell (c) is related to the fiber volume fraction by

$$c = h\sqrt{\frac{\pi\sqrt{3}}{6v_f}}. \tag{1}$$

A three-dimensional view of the composite is shown in Fig. 2. In the experiments presented in Vogler and Kyriakides (1997)[I] and in the preceding paper (Part I), the composite plate specimens were tested under essentially "plane strain" compression. This was achieved by clamping the specimen between two smooth steel plates. Post-failure examination of kink bands confirmed that the fibers inside them rotated only in the plane of loading (x_1–x_2 plane). Motivated by this, we impose a similar condition on the model by requiring the deformation to be quasi-planar. In addition, the net strain in the x_3-direction is required to be zero. Under these conditions, it becomes possible to limit attention to a characteristic slice of the material of thickness $(\sqrt{3}/2)c$ identified in Fig. 2. The two lateral surfaces of the slice are assumed to remain plane.

The micromechanical models used to study the onset of failure of such composites (Kyriakides et al., 1995; Kyriakides and Ruff, 1997[I]; Hsu et al. 1998) confirmed the suggestions of Argon (1972) and Budiansky (1983) that the critical load is a limit load instability strongly dependent on small fiber misalignments coupled with the nonlinearity of the composite response in shear (see also Budiansky and Fleck, 1993). Perhaps more importantly though, as a result of the more complete accounting of the characteristics of the material (axial stiffness, fiber bending stiffness, reasonably accurate spatial distribution of the fibers and matrix, accurate representation of the inelastic characteristics of the material, etc.) it became possible for the first time to follow the evolution of post-failure events. It was demonstrated that, following the limit load, deformation

[1] ()[I] Refers to figures and references in Part I.

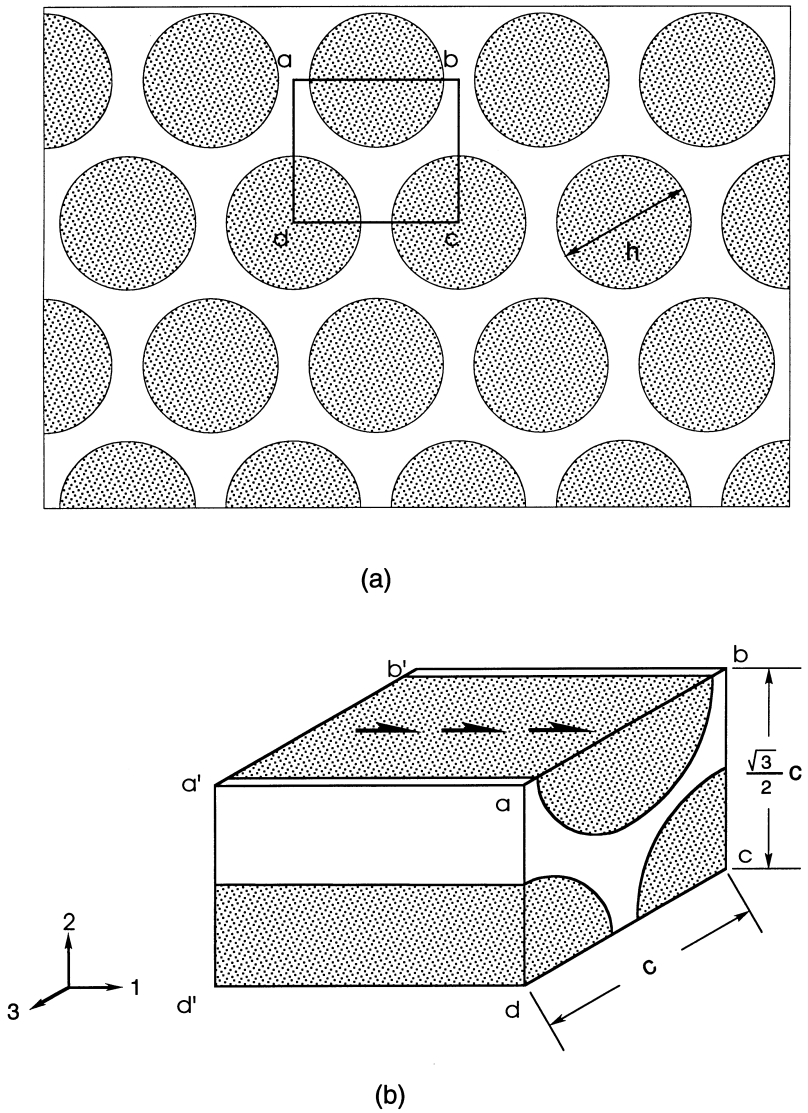

Fig. 1. (a) Composite idealized as a hexagonal array of round fibers in a PEEK matrix. (b) A representative cell for simulations of shearing response.

localizes into a narrow band of material which initially is essentially at 90° to the fibers ($\beta = 0$). Through the path-following quasi-static solution scheme used, the band was shown to simultaneously rotate and broaden while the overall load drops. In the process, the fibers develop ever increasing bending stresses at the edges of the band and eventually break. We suggested that it is perhaps this breaking of the fibers that locks in the "elusive" band angle β. For the model with the hexagonal fiber distribution, the band inclination and width corresponding to when fiber failure is expected were reasonably enough to give credence to this suggestion. On the other hand, some

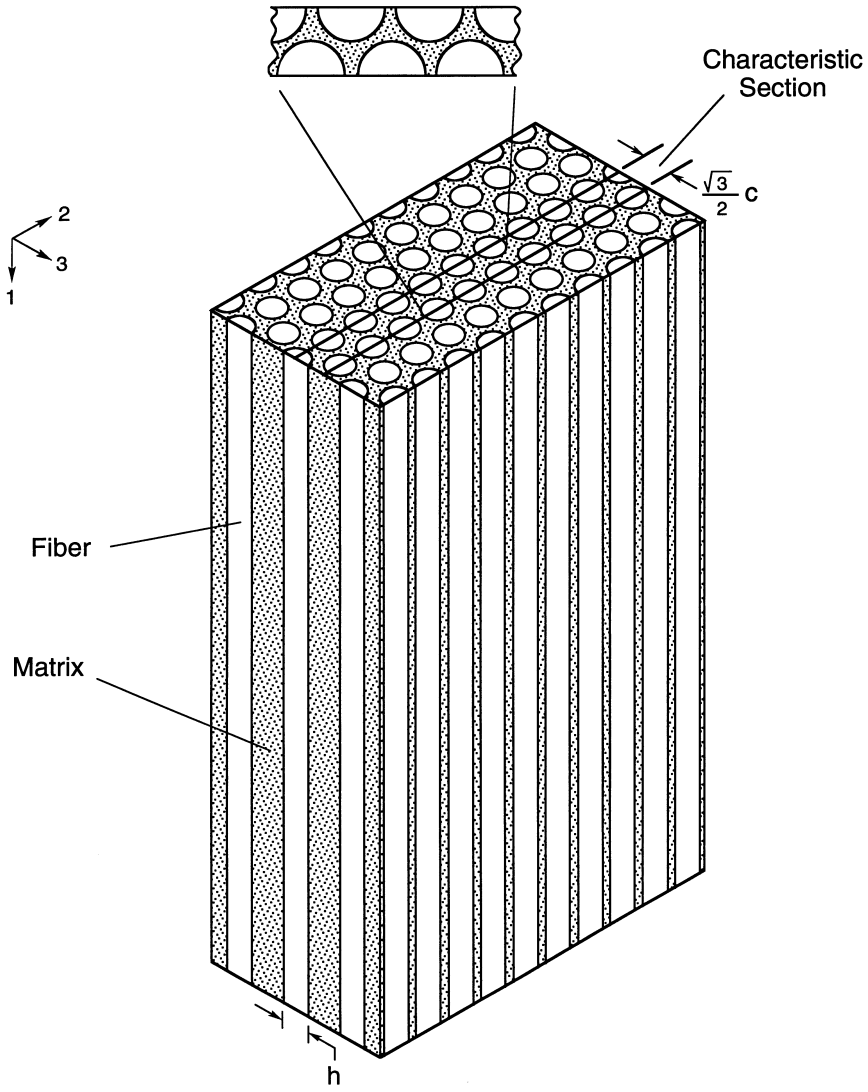

Fig. 2. A three-dimensional rendering of geometry of idealized composite.

fiber/matrix systems seem to kink without significant breaking of the fibers (Moran and Shih, 1998[1]; Fleck et al. 1997; unpublished results by Vogler and Kyriakides, 1997). Thus, other factors may play a role in setting the inclination of the band.

The quasi-static calculations also clearly showed the response to be highly unstable (characterized by limit and turning points) which explains why it has been so difficult to capture experimentally the formation of a kink band in uniformly loaded specimens like, for example, our rods and plates. In both types of specimens, we know that the band initiates at an edge due to the presence of a dominating imperfection and zips across the specimen at high speed. These, of course, are conditions which to date have not been simulated by any analysis. Thus, the exact evolution

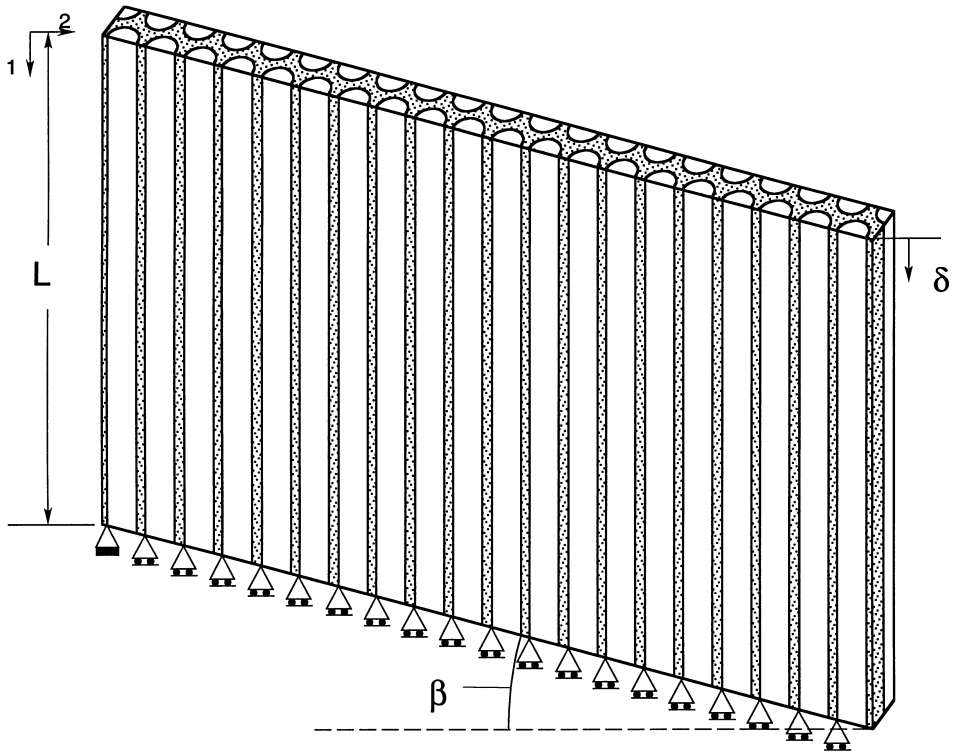

Fig. 3. Characteristic microsection of composite used for simulating axial propagation of kink bands.

of events that lead to the formation of a kink band with a well defined inclination remain somewhat vague. However, enough is known at this time to be able to say that the formation of the kink band is through a post-failure process of localization. As a result, we seriously doubt the chances of success in predicting the band inclination from just prefailure considerations of the composite as has been attempted by many authors (often motivated by success in predicting the inclination of the seemingly similar, but actually very different, inclined shear bands in metal strips in tension).

In the experiments we have performed on AS4/PEEK ($\bar{\beta} = 15.5^\circ$) but also IM8/PEEK ($\bar{\beta} = 11.5^\circ$) composites, the band inclination is so repeatable that, despite the difficulties in predicting its value described above, we have come to consider this angle a parameter characteristic of the material. Since the main objective of the present effort is not to model the onset of failure but rather to simulate steady-state propagation of a kink band which is already in place, in what follows the band inclination will be fixed a priori. Thus, the specimen analyzed has a lower edge with an initial inclination β as shown in Fig. 3. This can be thought of as the edge of a kink band which has already formed. The boundary conditions seen by the vertical fibers of the intact material are idealized as follows. The lower left point of each of the fibers in the strip analyzed is assumed to be hinged in a way that allows lateral movement as shown schematically in the figure. Rigid body motion is precluded by fixing one of the hinges in space.

An additional difference from the model in Hsu et al. (1998) is that the present model is assumed to be of infinite width. This is achieved numerically by requiring that fibers on each of the two

faces of the characteristic strip deform in a self-similar manner (details of this scheme are presented in the Appendix). This allows one to reduce the size of the domain analyzed to one of width of c (see Fig. 1(b)).

In order to adhere to the requirement of self-similar fiber deformation along the width, the upper edge of the strip is also made to be inclined (at an angle β to the x_2-axis) as shown in the figure. Thus, the domain is a parallelepiped of height L, thickness $(\sqrt{3}/2)c$ and width c. The strip is loaded by prescribing incrementally a uniform vertical displacement δ for all the nodes of the top surface. In order to reduce the initial load maximum exhibited during the initial transient part of the response, the whole microsection is made to have a 0.5° misalignment with the x_1-axis (this is computationally helpful but not necessary).

The domain is discretized with 20-node quadratic bricks and 15-node quadratic prisms within the framework of the nonlinear FE code ABAQUS[2] (full integration was used for both). The element distribution used to discretize the cross section is shown in Fig. 4(a). The microsection is made sufficiently tall ($L \sim 75h$) to allow development of steady-state propagation of the kink band. The elements in the fiber direction are more dense in the lower half of the domain (see Fig. 4(b)) as this is the area in which fiber kinking will take place. It is important to point that in the simulations that follow the fibers will bend but will not be allowed to break due to the very significant complication involved in such an undertaking. The implications of this deviation from the experimental facts will be discussed later in light of the results.

2.2. *Constitutive model*

As reported in Part I, the nonlinear behavior and rate dependence of the composite were examined through an extensive study which will be reported independently in the future. Here we limit attention on the pure shear behavior presented in Fig. 8[I] as we expect it to be the major player in determining the composite propagation stress. For the same reason we choose to model the matrix through the simplest possible inelastic model capable of reproducing the nonlinearity and rate dependence of the composite shear response, that is the powerlaw viscoplastic version of the J_2 flow rule. The simplicity of this model outweighs its inherent problem of plastic incompressibility known not to be appropriate for polymers such as PEEK.

The shear response recorded at $\dot{\gamma} = 10^{-3}\ \mathrm{s}^{-1}$ is selected as the baseline response for calibrating the elastic–viscoplastic model described below. The properties of the two constituents are obtained as follows. As in our previous work, the fibers are assumed to be linearly elastic and isotropic with the constants given in Table 1(a) (we adopt this knowing that the fibers are anisotropic because at this time the anisotropy of our AS4 fibers is not quantified). We use these fiber properties in the pure shear micromodel shown in Fig. 1(b) to calculate the matrix properties required so that the τ_{12}–γ_{12} response from the model matches, as well as possible, the measured shear response in Fig. 5(a). In this calibration calculation, the matrix is assumed to be a J_2 flow theory solid which hardens isotropically. The micromodel is sheared by fixing the surface $cdd'c'$ and displacing uniformly the surface $abb'a'$ as indicated in Fig. 1(b) while requiring that the surfaces $abcd$ and $a'b'c'd'$ deform in a self-similar manner.

---

[2] We are grateful to Hibbitt, Karlsson and Sorensen, Inc. for making ABAQUS available under academic license.

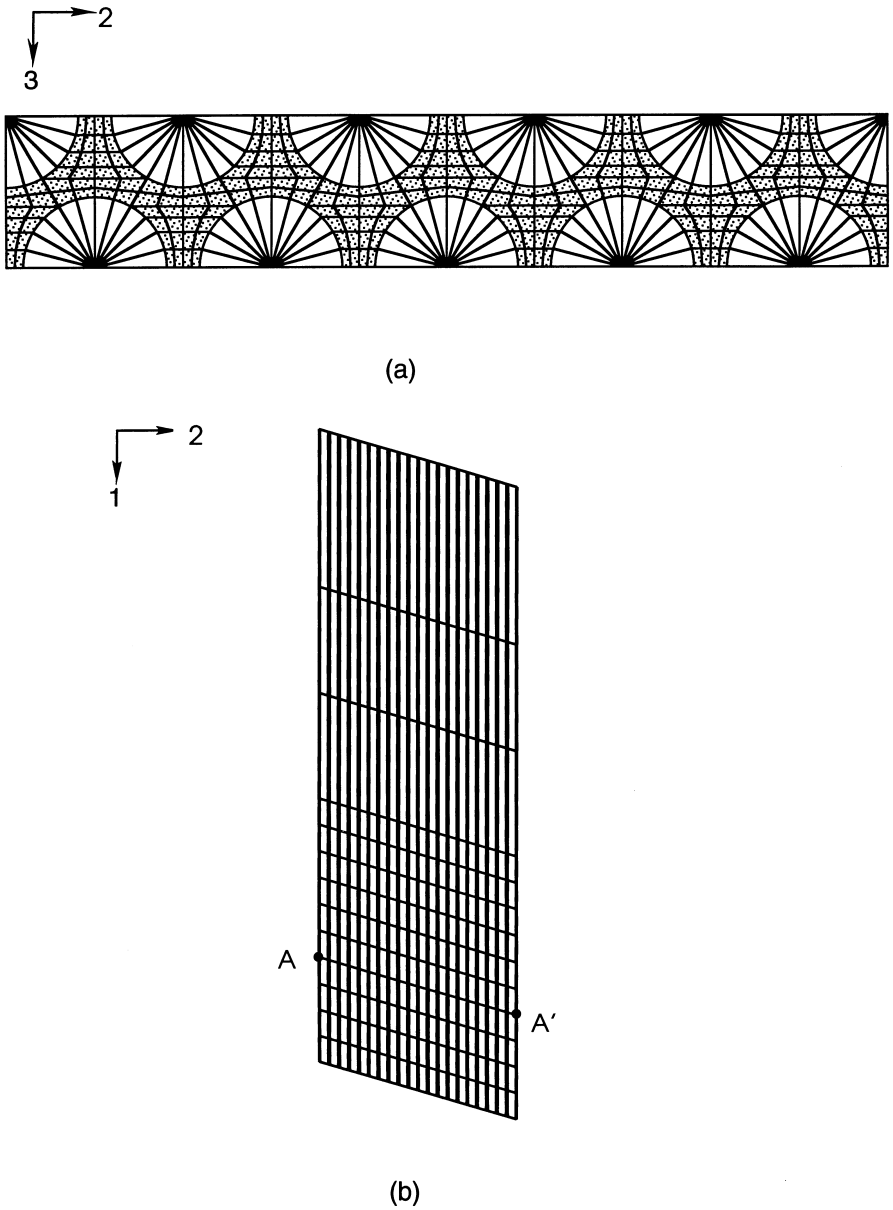

Fig. 4. FE discretization of micromodel.

The best fit response calculated is shown with a dashed line in Fig. 5(a). The matrix stress–strain response which yielded this fit is shown in Fig. 5(b). In Hsu et al. (1998) we pointed out that when the measured stress–strain response of neat PEEK was used in a similar calculation, the predicted shear response was in good agreement with measured results in the elastic range and up to a strain of approximately 1.5%. Subsequently, it underpredicted the experimental results. PEEK is a

Table 1. Mechanical properties of composite constituents

(a)

AS4 Fibers	
E_f msi (GPa)	v_f
31.0 (214)	0.263

(b)

APC-2 (PEEK) Matrix				
E_m ksi (GPa)	v_m	σ_{0m} (MPa)	$\dot{\varepsilon}_0$ s^{-1}	m
594 (4.10)	0.356	3.9 (27)	2.5×10^{-3}	0.020

semicrystalline polymer and is thought to crystallize differently in the composite due to the presence of the fibers (see Jar et al., 1992). The thermal history is known to affect PEEK also (Cebe et al., 1987). Both of these factors are suspected to contribute to this difference. Accurate prediction of the shear response up to 1.5% was sufficient for establishing the onset of failure, the main concern of Hsu et al. (1998). In the present problem, the large strain response of the material is of paramount interest. Thus, use of the neat properties was no longer an acceptable option, and they were replaced by the in situ stress–strain response extracted in the manner described above. The difference between the neat and in situ responses can be seen in Fig. 5(b).

The basic features of the elastic–viscoplastic model used for the matrix are as follows. Strain increments are assumed to consists of an elastic part and an inelastic part

$$\underline{\dot{\varepsilon}} = \underline{\dot{\varepsilon}}^e + \underline{\dot{\varepsilon}}^p. \tag{2}$$

Elastic deformations are linear and isotropic and are related to stresses by

$$\underline{\dot{\varepsilon}}^e = \frac{1+v_m}{E_m}\underline{\dot{\sigma}} - \frac{v_m}{E_m}\mathrm{tr}(\dot{\sigma})\underline{I} \quad \text{or} \quad \underline{\dot{\sigma}} = \underline{C}(E_m, v_m)\underline{\dot{\varepsilon}}^e \tag{3}$$

where the Young's modulus (E_m) and the Poisson's ratio (v_m) are assumed to be independent of rate (values given in Table 1(b)).

The inelastic part of the deformation ($\underline{\dot{\varepsilon}}^p$) is assumed to exhibit a simple power law rate dependence (Nadai, 1950), which for a uniaxial state of stress is given by

$$\left(\frac{\dot{\varepsilon}^p}{\dot{\varepsilon}_0}\right)^m = \frac{\sigma}{\Sigma(\varepsilon^p)}. \tag{4}$$

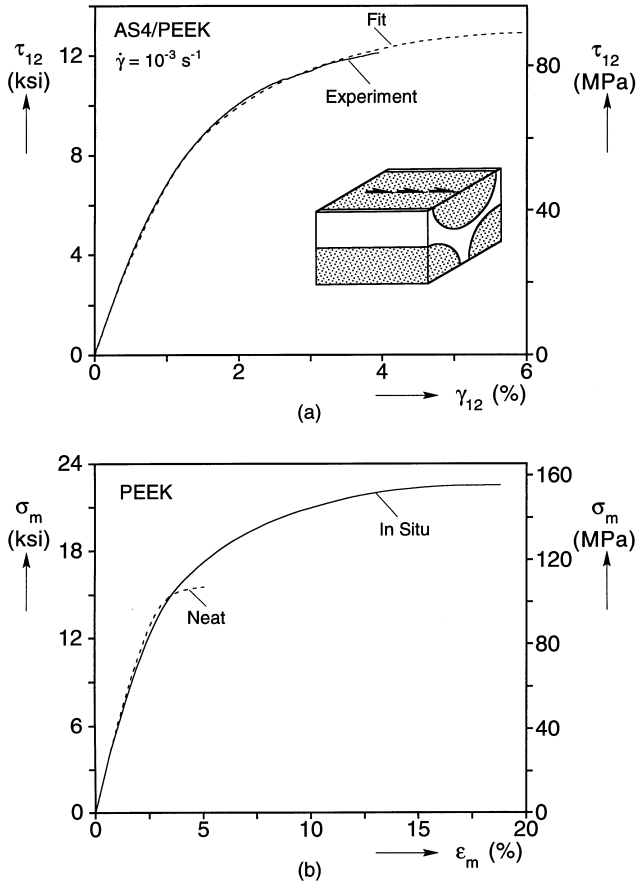

Fig. 5. (a) Measured shear response of AS4/PEEK and fit. (b) Comparison of stress–strain responses of neat and *in situ* PEEK.

Here, $\dot{\varepsilon}_0$ is a reference strain rate, $\Sigma(\varepsilon^p)$ is the flow stress measured when $\dot{\varepsilon}^p = \dot{\varepsilon}_0$, and m is the rate exponent. The yield stress (σ_{0m}) was selected to be 3.9 ksi (26.9 MPa) and the inelastic part of the response was fitted with a multilinear fit (48 segments of variable strain spans). The value of the rate exponent was found in the usual way to be 0.020 from a set of compression tests on neat PEEK cylinders tested at strain rates in the range $10^{-4} \leqslant \dot{\varepsilon} \leqslant 10^{0}$.

The model was generalized to the multiaxial setting through the classical associative plasticity framework (e.g., see Peirce et al., 1984). The plastic strain rate is given by

$$\underline{\dot{\varepsilon}}^p = \Lambda \frac{\partial f}{\partial \underline{\sigma}} \tag{5}$$

with the following choice for f:

$$f = \sigma_e = \sqrt{\tfrac{3}{2}\underline{s}\cdot\underline{s}}, \quad \underline{s} = \underline{\sigma} - \tfrac{1}{3}(\mathrm{tr}\,\underline{\sigma})\underline{I}. \tag{6}$$

A work compatible measure of equivalent strain rate is given by

$$\dot{\varepsilon}_e^p = \sqrt{\tfrac{2}{3}\underline{\dot{\varepsilon}}^p \cdot \underline{\dot{\varepsilon}}^p}. \tag{7}$$

Substituting (4), (6) and (7) →(5) yields

$$\underline{\dot{\varepsilon}}^p = \dot{\varepsilon}_e^p \left(\frac{3}{2}\frac{\underline{s}}{\sigma_e}\right) = \dot{\varepsilon}_0 \left(\frac{\sigma_e}{\Sigma(\varepsilon_e^p)}\right)^{1/m} \left(\frac{3}{2}\frac{\underline{s}}{\sigma_e}\right) \tag{8}$$

where

$$\varepsilon_e^p = \int_0^t \dot{\varepsilon}_e^p \, \mathrm{d}t. \tag{9}$$

By combining (3) and (8) through (2) and inverting we arrive at

$$\underline{\dot{\sigma}} = \underline{\underline{C}}\,\underline{\dot{\varepsilon}} - \left(\frac{3\dot{\varepsilon}_e^p}{2\sigma_e}\right)\underline{\underline{C}}\,\underline{s}. \tag{10}$$

For numerical expediency, the value of $\dot{\varepsilon}_e^p$ in a given time increment (Δt) was evaluated through the forward gradient method (Peirce et al., 1984). This method linearly interpolates the values of $\dot{\varepsilon}_e^p$ at t and $t+\Delta t$ as follows:

$$\frac{\Delta\varepsilon_e^p}{\Delta t} = [(1-\xi)\dot{\varepsilon}_e^p|_t + \xi\dot{\varepsilon}_e^p|_{t+\Delta t}] \tag{11a}$$

where $\xi(\in[0,1])$ is a numerical parameter selected for optimum performance and

$$\dot{\varepsilon}_e^p|_{t+\Delta t} = \dot{\varepsilon}_e^p|_t + \frac{\partial\dot{\varepsilon}_e^p}{\partial\sigma_e}\Delta\sigma_e + \frac{\partial\dot{\varepsilon}_e^p}{\partial\varepsilon_e^p}\Delta\varepsilon_e^p. \tag{11b}$$

In the present problem, $\xi = 0.5$ was found to yield optimum results. (An extensive evaluation of this model for simulating complex loading histories of another polymer can be found in Papka and Kyriakides, 1998, where the model was used with success in an analysis of crushing of a polycarbonate honeycomb.)

The last variable of the model to be determined was the strain rate of the base response ($\dot{\varepsilon}_0$). This was established through an iterative process as follows. The constitutive model with the material parameters given in Table 1 along with the matrix stress–strain response in Fig. 5(b) (solid line) was used to conduct a simulation of a pure shear test on the micromodel shown in Fig. 1(b). The test was conducted at an average rate of $\dot{\gamma} = 10^{-3}\ \mathrm{s}^{-1}$. During the first iteration, $\dot{\varepsilon}_0$ was assigned a best guess value. An updated guess was produced depending on whether the calculated response was higher or lower than the one measured. The process was repeated until the calculated response matched the experimental one. In this converged "solution" $\dot{\varepsilon}_0 = 2.5\times10^{-3}\ \mathrm{s}^{-1}$. This value was found to be in good agreement with the mean value of the strain rates at the integration points in the matrix when the plateau stress is reached.

The fully calibrated constitutive model was then used in the pure shear micromodel to reproduce the set of composite shear responses in Fig. 8[I]. The predicted responses are compared to those

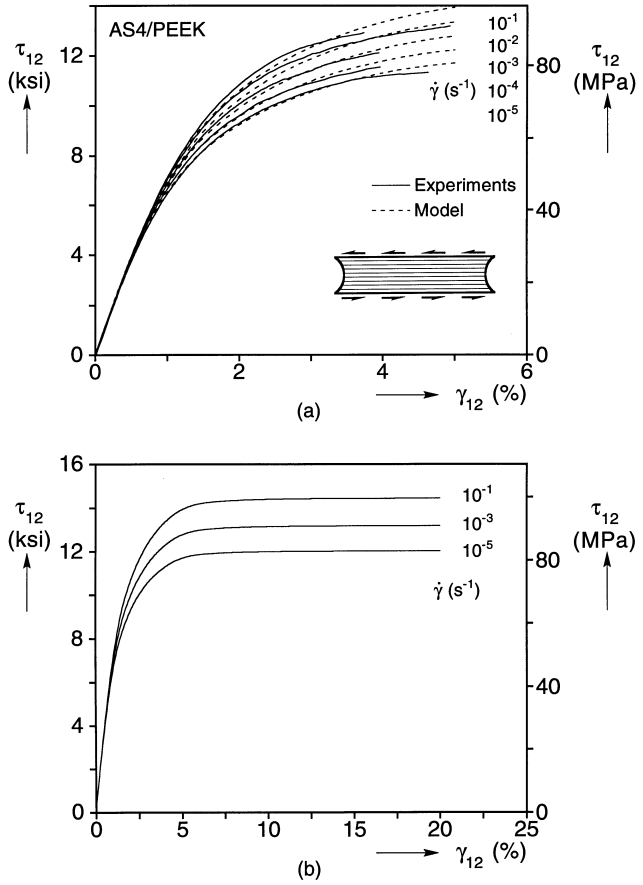

Fig. 6. (a) Comparison of measured and predicted shear responses at different strain rates. (b) Model shear responses at large strains.

measured in Fig. 6(a). The predictions are seen to be in reasonably good agreement with the measured results for all strain rates. Interestingly, the rate exponent predicted for the composite was found to correspond very closely to that of the matrix.

One last constitutive issue must be addressed before moving on to the simulation of steady-state broadening of kink bands. The experiments have clearly demonstrated that the shear deformation in the kink band reaches values as high as 40°. Since our shear experiments terminated at strains of the order of 5–6%, we do not know exactly the material response at the large shear angles of interest. We arbitrarily extrapolated the basic shear response in Fig. 5(a) so that at a strain of 7% it smoothly reaches a stress plateau of 12.98 ksi (89.5 MPa). This results in a stress plateau in the *in situ* matrix of 22.5 ksi (155 MPa) which is achieved after a strain of 18.8%. With these additional assumptions, the composite shear response predicted by the model at shear strain rates spanning five decades are illustrated in Fig. 6(b). A stress plateau is seen to develop at larger shear strains for all three cases shown.

It should be pointed out that during the bend–break–rotate process experienced by the deforming

zone adjacent to the band, the material undergoes a complex loading history which includes shear and transverse stresses. In the early stages of bending, the transverse stresses are tensile but subsequently become compressive. Thus, transverse cracking or some other form of damage cannot be precluded in practice. In the experiments, transverse cracking was not observed; thus, if cracks did form they must have closed when the transverse stress switched to compression. This possible complication will not be considered in our model.

3. Simulation of kink band propagation

3.1. *Kink band propagation at* $\dot{\delta}/\mathrm{h} = 0.5\ s^{-1}$

The main characteristic dimension of the problem is the fiber diameter h ($=7\ \mu$m—0.28×10^{-3} in). Thus, h will be used to normalize other dimensions. The first microsection analyzed has a height $L = 75h$ and its edges are inclined at 15°. The microsection is loaded at a constant prescribed end-displacement rate ($\dot{\delta}$) very much like in the experiment. In order to match the experimental conditions closely, two different displacement rates will be used. Initially (initiation stage), when the deformation in the microsection is uniform, a slower displacement rate of $\dot{\delta}/h = 5.4\times10^{-3}\ \mathrm{s}^{-1}$ is used. This results in a strain rate which matches that of our 1.86 in (46.2 mm) tall plate during the initiation phase of the test. Subsequently, when the deformation localizes, the displacement rate is switched to a value that corresponds to that used in the particular experiment being simulated. The displacement supplied now goes entirely into the kink band and, as a result, the difference in height between the plate tested and the micromodel analyzed is no longer relevant.

Figure 7 shows a typical stress-end shortening response produced where

$$\dot{\delta}(t) = \int_0^t \ddot{\delta}\,\mathrm{d}t \tag{12}$$

and $\sigma_{11}(t)$ is the corresponding average stress at the top surface of the microsection. The initial (⓪) and a set of deformed configurations corresponding to the points on the response identified by numbered solid bullets, are included in the figure. The microsection initially deforms elastically. Plastification of the matrix leads to a load maximum, and subsequently deformation is seen to localize at the lower edge of the microsection. The value of the load maximum is characteristic of the particular setup we use and has no other useful meaning. Although the eccentric hinging of the fibers at the lower edge is sufficient disturbance to initiate the localized deformation, by misaligning all the fibers by 0.5° the value of the load maximum is reduced further. It is important to point out that, as is the case for other propagating instabilities (Kyriakides, 1994), such details (method of hinging of fibers, fiber misalignment angle, etc.) affect the initiation load but have no effect on the steady-state propagation process.

The localized deformation is in the form of local bending of a strip of fibers at the lower edge clearly seen in configuration ①. Localization progresses with a net drop in the mean stress. In the neighborhood of equilibrium point ①, the end displacement rate is increased to $\dot{\delta}/h = 5\times10^{-1}$ s^{-1}, that is, a value corresponding to the rate of the experiment in Figs 3[I]–6[I]. A small local stress peak develops as a result of this sudden increase in rate, but the response reverts quickly to its downward trajectory. By configuration ②, the "knee" of bent fibers has moved away from the

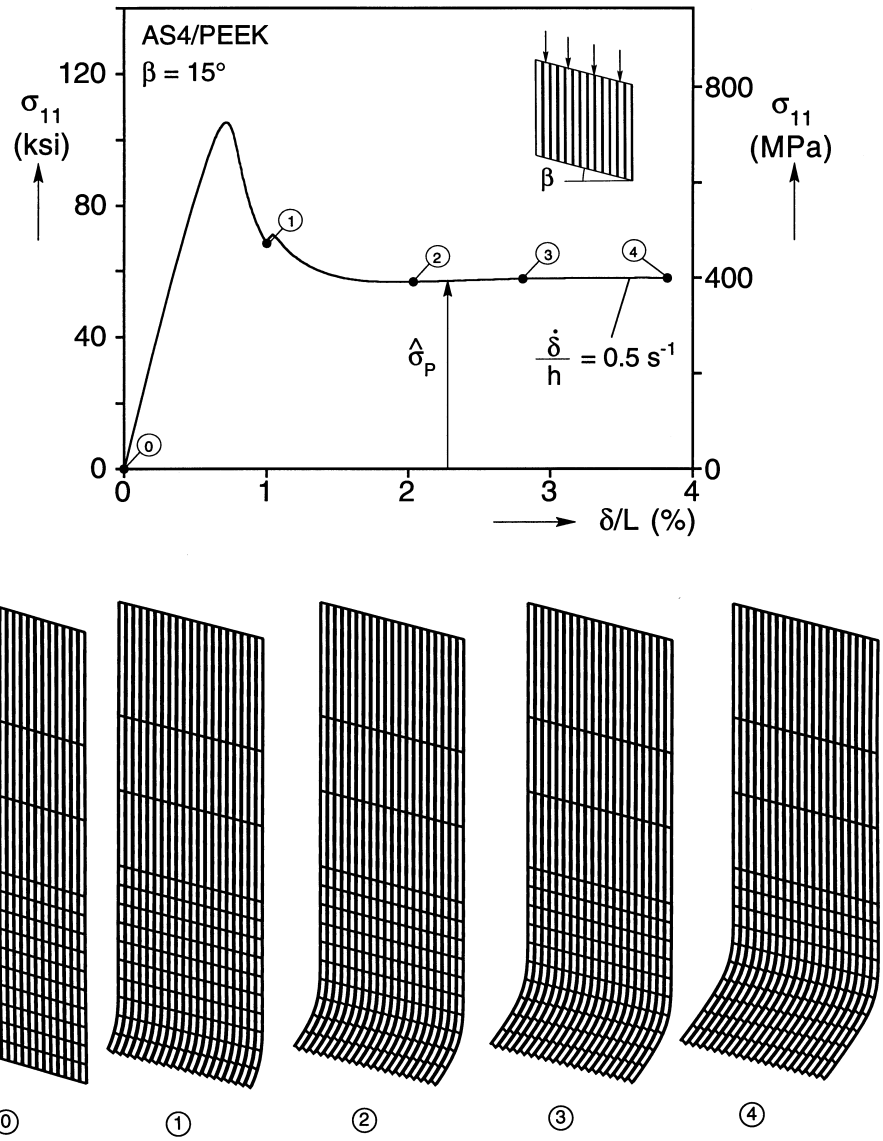

Fig. 7. Numerical simulation of axial propagation of a kink band. (a) Axial stress-end shortening response. (b) Sequence of configurations of the microsection analyzed.

lower edge. We now have two distinct zones: a zone of rotated but straight fibers at the lower end and a zone of straight fibers at the upper end. The two are joined by a transition zone of bent fibers (the knee) which has a width of the order of $10h$. As displacement is supplied at the top end, the width of the bent zone of fibers grows and the knee moves upwards, essentially unaltered. Thus, a steady-state process has been reached and this is reflected by the stress plateau that develops in the response. In the experiments, although most of the bent fibers broke into small

segments, zones of bent but unbroken fibers could be found at the edges of kink bands. The size and curvatures of these bent zones are similar to those seen in Fig. 7.

The plateau stress represents the propagation stress ($\hat{\sigma}_P$) of the problem as set up. At this displacement rate, $\hat{\sigma}_P = 58$ ksi (400 MPa) which compares with a mean value at 69.6 ksi (480 MPa) measured in the eight experiments reported in Part I and a range of 61–77 ksi (421–531 MPa). The fibers in the bent zone rotate to 36.8° ($\hat{\phi}_P$) which compares with a mean value of 40.5° measured directly in four experiments and a range of 40–42°. That is, the model composite is less compliant. Possible reasons for this are: the fibers in the model are not allowed to break, the plastic deformation of the matrix was assumed to be volume preserving which is known not to be exactly correct for this polymer, and transverse microcracks or some other form of material damage may take place in practice but were not allowed in the model. These issues may have also contributed to lowering the predicted propagation stress. We suspect, however, that the latter may be more related to a rather low choice made for the value of the plateau stress for the shear response of the composite. Order-of-magnitude calculations of the energy expended to create new surfaces due to the breaking of the fibers into fragments of the order of $10h$, indicate that this contribution is relatively small. Therefore this should not significantly affect $\hat{\sigma}_P$.

3.2. *Parametric study of propagation stress*

The micromodel was subsequently used to conduct a limited parametric study of the propagation stress. In the present work the kink band inclination β is prescribed. We thus conducted a series of calculations in which β was varied from 11–19° at two degree intervals. The calculated propagation stresses and the corresponding fiber rotation angles are listed in Table 2. The propagation stress is seen to decrease from 69.3 ksi (478 MPa) at $\beta = 11°$ to 50.3 ksi (347 MPa) at $\beta = 19°$. Correspondingly, $\hat{\phi}_P$ increases from 32.7–41.8°.

Table 2. Effect of kink band inclination on predicted propagation stress and fiber rotation ($\dot{\delta}/h = 5 \times 10^{-1}\ \mathrm{s}^{-1}$)

β^0	$\hat{\phi}_P^\circ$	$\hat{\sigma}_P$ ksi (MPa)
11	32.7	69.3 (478)
13	34.6	63.1 (435)
15	36.8	58.0 (400)
17	39.2	53.7 (370)
19	41.8	50.3 (347)

Table 3. Effect of level of ultimate stress of shear response of propagation stress

Case	τ_u ksi (MPa)	$\hat{\sigma}_P$ ksi† (MPa)	(τ_u/τ_{u2})	$(\hat{\sigma}_P/\hat{\sigma}_{P2})$
1	12.0 (82.8)	53.2 (367)	0.923	0.917
2	13 (89.7)	58.0 (400)	1.0	1.0
3	14.3 (98.6)	63.0 (434)	1.1	1.086

† $\dot{\delta}/h = 5 \times 10^{-1}\ \mathrm{s}^{-1}$.

As indicated earlier, there is some uncertainty about the level of the stress plateau (τ_u) in the shear response in Fig. 6(a). For this reason, we examined the sensitivity of the propagation stress on this parameter as follows. The matrix stress–strain parameters were varied to produce composite shear responses of three ultimate stress levels (at the base rate of $\dot{\gamma} = 10^{-3}\ \mathrm{s}^{-1}$). The three levels of τ_u are listed in Table 3. The one corresponding to case 2 is the same value to produce the results in Fig. 7. The matrix stress–strain responses generated in this fashion were then used in the kink band propagation FE model. The propagation stresses calculated for each of the three material responses are listed in Table 3. Changing of τ_u is seen to produce a corresponding change in $\hat{\sigma}_P$.

The two variables τ_u and $\hat{\sigma}_P$ for cases 1 and 3 were then normalized with the corresponding values of case 2. We observe that, at least in the range of τ_u considered, the change in $\hat{\sigma}_P$ is almost identical to the change in τ_u, or in other words, $\hat{\sigma}_P$ scales with τ_u. Since we believe that the extrapolation of the base shear response we used is probably a lower bound of the actual response, if σ_P scales with τ_u our predictions of the propagation stress can also be considered lower bound estimates.

Recently Budiansky et al. (1997)[I] produced a relatively simple expression for estimating $\hat{\sigma}_P$. The essence of their model is as follows. The kink band is assumed to propagate in a steady-state manner by a unit distance. The external work done by the applied stress is calculated and equated to an estimate of the internal energy expended due to the shearing of the kink band. The composite is assumed to be rate independent which yields the following expression for the propagation stress

$$\hat{\sigma}_P(\beta, \phi_{\max}) = \frac{\int_0^{\phi_{\max}} \tau(\phi)\cos(\beta-\phi)\,\mathrm{d}\phi}{\cos\beta(1-\cos\phi_{\max})}. \tag{13}$$

In their calculations $\phi_{\max}$ was assumed to be 2β. Moran et al. (1995)[I] developed a similar expression for $\hat{\sigma}_P$ with two differences. First, they assumed that the shear response is initially elastic-perfectly plastic but hardens when the shear strain reaches a certain value ($\gamma \sim 0.3$); second, the metric introduced in (13) to account for finite deformations was neglected.

We use this expression to establish trends for $\hat{\sigma}_P$ similar to the ones derived via our model. To make the comparison of the result of eqn (13) with those obtained numerically meaningful, in

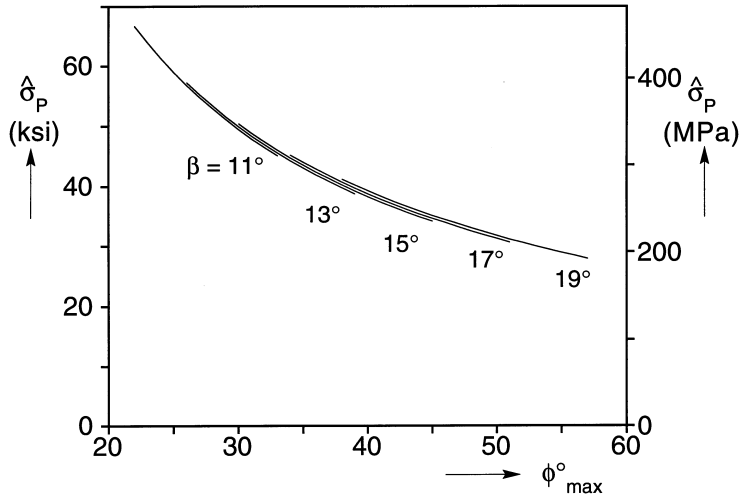

Fig. 8. Propagation stress predicted using eqn (13) for various values of band inclination β and maximum fiber rotation ϕ_{max}.

place of $\tau(\phi)$ we use the extrapolated shear response of the composite for $\dot{\gamma} = 10^{-3}\ s^{-1}$ (Fig. 5(a)) but neglect its rate dependence. The integration is then performed numerically. In addition, in view of the evidence to the contrary reported in Part I, we will relax the assumption that $\phi_{max} = 2\beta$.

We first examine the sensitivity of $\hat{\sigma}_P$ to the two important variables β and ϕ_{max}. We vary β from 11–19° at two degree intervals and in each case we calculate $\hat{\sigma}_P$ for $2\beta \leqslant \phi_{max} \leqslant 3\beta$. The results are shown in Fig. 8. For all values of β considered, the propagation stress is seen to drop as ϕ_{max} is increased.

We now perform a direct comparison of the predictions of $\hat{\sigma}_P$ from eqn (13) with those yielded by our FE model. Two sets of predictions are made using (13). First, the propagation stress is calculated for various values of β by adhering to the assumption that $\phi_{max} = 2\beta$. The same calculations are then repeated, but this time we assign ϕ_{max} the value found in the corresponding run of the FE model (given in Table 2). The results are shown in Fig. 9. The FE results clearly indicate that the propagation stress drops as β is increased. Both sets of results from eqn (13) capture this trend, which is reassuring. However, the more realistic of the two sets of predictions, that is, the one for $\phi_{max} = \hat{\phi}_P$, is rather low by comparison to the FE predictions.

The case of $\beta = 15°$ is the one which corresponds to the experiments reported in Part I. The mean values and the range measured for variables β, σ_P and ϕ_P are listed once more in Table 4. Included are the corresponding predictions from the FE model and those of eqn (13) for ϕ_{max} of 30 and 36.8°. The FE predictions are somewhat lower than the experimental results possible for the reasons given above. The value of σ_P yielded by eqn (13) is quite a bit lower than the FE predictions when the more realistic value of ϕ_{max} is used. The prediction will become even lower if the fiber rotation angle is given the experimental value 40.5°. This indicates that changing the value of ϕ_{max} used in (13) to one more representative of the value measured at the propagation stress is not the most appropriate way to improve the performance of this model. A modification which includes a more realistic representation of the mechanism through which the deformation inside

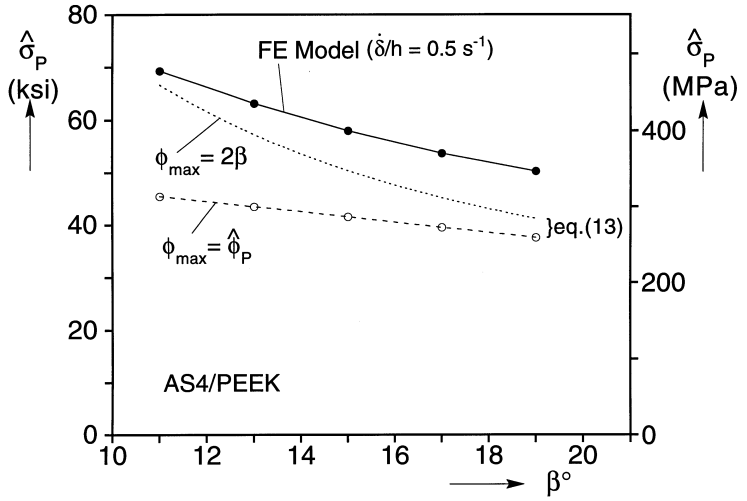

Fig. 9. Comparison of propagation stresses predicted by the FE model and eqn (13).

Table 4. Comparison of measured and predicted values of propagation stress

	Experiments	FE Model*	Eqn (13)	Eqn (13)
β°	15.5† 13–17‡	15	15	15
ϕ_P°	40.5† 40–42‡	36.8	30	36.8
σ_P ksi (MPa)	69.6 (480)† 61–77 (421–531)‡	58.0 (400)	50.4 (348)	41.5 (286)

* $\dot{\delta}/h = 5 \times 10^{-1}\ \mathrm{s}^{-1}$.
† Mean value.
‡ Range.

the kink band is arrested should be explored. Interestingly, eqn (13) yields correctly the proportionality of σ_P to τ_u found from our results see also eqn (24) in Budiansky et al. 1997[I]).

3.3. *Effect of rate on the propagation stress*

The FE model is now used to examine the effect of the displacement rate $\dot{\delta}$ on the calculated propagation stress, adhering to the procedure followed in the experiments (Part I). The kink band inclination is fixed at 15°. The band is initiated very much in the fashion described in the previous section ($\dot{\delta}/h = 5.4 \times 10^{-3}\ \mathrm{s}^{-1}$). When deformation localizes and the load starts to drop, the displacement rate is switched to the desired value. Steady-state band propagation is reached and, as a result, a well defined stress plateau is traced. Following this, the displacement rate is changed by

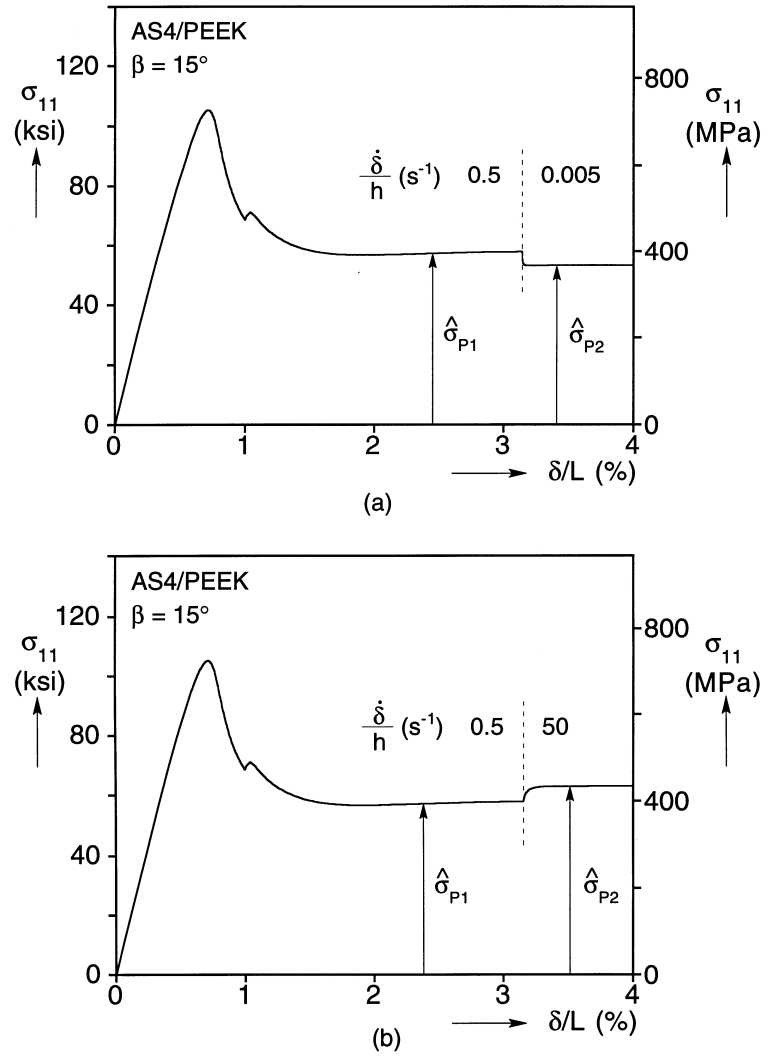

Fig. 10. Axial stress-end shortening response for simulations in which the loading rate was (a) decreased and (b) increased by two decades during the steady-state propagation.

two decades. The response experiences a small transient but eventually stabilizes to a new stress plateau and a new steady-state condition develops.

Sample results from such simulations are shown in Fig. 10. Figure 10(a) shows the response from a simulation in which the band is first propagated at a rate of $\dot{\delta}/h = 5 \times 10^{-1}$ s^{-1}. The propagation stress is at the same level as in the case presented in Fig. 7 (see Table 5). When the overall shortening of the specimen reaches 3%, the rate at which the specimen is compressed is reduced by two decades. Following a brief transient, the propagation stress is seen to drop to a lower level of 53.3 ksi (368 MPa). Interestingly, the rotation of the fibers inside the kink band decreases by approximately half a degree, presumably due to the lower stress.

Table 5. Effect of end displacement rate on predicted propagation stress and fiber rotation ($\beta = 15^\circ$)

$(\dot{\delta}/h)$ s^{-1}	$\hat{\phi}_P^\circ$	$\hat{\sigma}_P$ ksi (MPa)
5×10^{1}	37.2	63.0 (434)
5×10^{-1}	36.8	58.0 (400)
5×10^{-3}	36.4	53.3 (368)

The first part of the response shown in Fig. 10(b) is the same. The first plateau stress is the one corresponding to $\dot{\delta}/h = 5 \times 10^{-1}\ s^{-1}$. In this case when $\delta/L = 0.03$ the displacement rate is increased by two decades. As a result, we see the propagation stress increase to 63 ksi (434 MPa) while simultaneously $\hat{\phi}_P$ increased by approximately one half of a degree. Thus, we see that a two decade change in the displacement rate has the result of increasing or decreasing the calculated propagation stress by approximately 10% as was the case in the experiments.

In the previous section we examined the effect of the ultimate stress of the composite base shear response τ_u and σ_P. The three levels of τ_u used in those calculations were purposely chosen to be the same as those obtained by changing the shear strain rate by two decades from the base value of $\dot{\gamma} = 10^{-3}\ s^{-1}$ (Fig. 6(b)). It is interesting to observe that the calculated values of σ_P in Table 5 are very similar to the three values listed in Table 3. In other words, changing the loading rate two decades has the same effect on σ_P as shifting τ_u the same amount as a two decade change in $\dot{\gamma}$ induces.

4. Conclusions

A micromechanical model of axial propagation (broadening) of kink bands in fiber/matrix composites has been presented. The model is used to simulate steady-state propagation of an existing kink band inclined at a prescribed angle β to the x_2-axis of the composite. The material is idealized as a hexagonal array of round elastic fibers in an elastic-powerlaw viscoplastic matrix. Since deformation is known to be planar (Part I), it was possible to limit attention to a characteristic slice of the material. The slice is made to behave as if it were infinitely wide by imposing periodicity conditions on the sides of the micromodel used. The model deviates from the experimental observations in that the fibers are allowed to bend but not to break.

An important ingredient of the model is the calibration of the elastic–viscoplastic constitutive model used for the matrix. The *in situ* properties of the PEEK matrix were extracted by matching simulations of pure shear to experimental data for the AS4/PEEK composite. The *in situ* properties were found to be different from properties measured in neat matrix. The rate exponent m of the matrix was determined to be 0.020 from a series of compression tests at various strain rates on

neat PEEK. The constitutive model was shown to reproduce successfully the rate independence of the composite shear response over a shear strain rate range spanning five decades.

The micromechanical model was used to calculate the propagation stress of the composite at various end displacement rates. For the base rate of $\dot{\delta}/h = 5 \times 10^{-1}\,\mathrm{s}^{-1}$, the calculated propagation stress was 58 ksi (400 MPa) compared with a mean value from eight experiments of 69.6 ksi (480 MPa) and a range of 61–77 ksi (421–531 Mpa). The calculated fiber rotation angle inside the kink band was 36.8° which compares with a 40.5° average value measured. Part of the difference in the calculated propagation stress is attributed to some uncertainty in the plateau stress assumed for the composite shear response at large shear strains. The model was found to accurately reproduce the effect of rate of compression on the propagation stress. A change of two decades in the applied end displacement rate produces a 10% change in the propagation stress. This agrees well with the experimental results in Part I.

A limited parametric study was performed with the current model and one recently developed by Budiansky et al. (1997)[I]. The propagation stress was found to scale with the plateau stress of the shear response for both models. The simpler model was found to be useful for evaluating trends in σ_P. We expect its quantitative accuracy to be improved when a more realistic representation of the mechanism through which the deformation inside the kink band is arrested is incorporated.

Acknowledgements

The financial support of the Office of Naval Research under contract N00014-97-1-0515 is acknowledged with thanks. The work of TJV was also supported by the Fannie and John Hertz Foundation and the W. M. Keck foundation.

Appendix: Periodicity conditions for micromodel

The kink band was modeled to be of infinite width by imposing the following periodicity conditions. The displacements of nodes on the right side of the micromodel are related to the displacements of their counterparts on the left side as follows. Consider node A on the LHS of the model and the corresponding node A′ on the RHS (see Fig. 4(b)). Vertical (x_1) and out-of-plane (x_3) displacements of A and A′ nodes are constrained to be the same. The horizontal (x_2) displacements of the nodes are related in such a way as to allow a uniform transverse strain in the composite. Thus, they are related by:

$$\mathrm{u}_2(\mathrm{A}') = \mathrm{u}_2(\mathrm{A}) + \varepsilon_t \mathrm{b} \tag{A1}$$

where ε_t is the uniform transverse strain of the composite and b is the width of the section modeled. The other nodes on the two vertical sides of the micromodel are treated in the same fashion. Note that the value of ε_t is not prescribed; rather, it is determined by the FE calculation.

References

Argon, A., 1972. Fracture of composites. In Treatise of Materials Science and Technology 1, 79–114.

Budiansky, B., 1983. Micromechanics. Computers and Structures 16, 3–12.

Budiansky, B., Fleck, N.A., 1993. Compressive failure of fibre composites. Journal of the Mechanics and Physics of Solids 41, 183–211.

Cebe, P., Hong, S.-D., Chung, S., Gupta, A., 1987. Mechanical properties and morphology of poly(etheretherketone). Toughened Composites, ASTM STP 937, ed. N. J. Johnston, pp. 342–357. ASTM, Philadelphia.

Hsu, S.-Y., Vogler, T.J., Kyriakides, S., 1998. Compressive strength predictions for fiber composites. ASME Journal of Applied Mechanics 65, 7–16.

Jar, P.-Y., Cantwell, W. J., Kausch, H.H., 1992. Study of crystal morphology and the deformation behaviour of carbon fibre reinforced PEEK (APC-2) Composites Science and Technology 43, 299–306.

Kyriakides, S., 1994. Propagating instabilities in structures. In Advances in Applied Mechanics, ed. J. W. Hutchinson and T. Y. Wu, 30, 67–189. Academic Press, Boston, MA.

Nadai, A., 1950. Theory of Flow and Fracture of Solids. Vol. I, 2nd edn. McGraw-Hill, New York.

Papka, S. D., Kyriakides, S., 1998. In-plane crushing of a polycarbonate honeycomb. International Journal of Solids and Structures 35, 239–267.

Peirce, S.D., Shih, C.F., Needleman, A., 1984. A tangent modulus method for rate dependent solids. Computers and Structures 18, 875–887.